the spontaneous baroreflex method, the analytical time window based on short-time FFT[5] (STFFT) has been adjusted to evaluate the time-varying gain around the operating point. However, this method may not be suitable for the evaluation of short-term changes in baroreflex properties for AP regulation through sympathetic as well as vagal nerves, at multiple pressure points with background noise. A combination of time and frequency analysis using wavelet transform may be able to identify the dynamic baroreflex properties efficiently regardless of background noise[2,4] by virtue of its high temporal resolution.[34] If dynamic and static characteristics in cardiovascular patients with unstable hemodynamics can be identified in a short-duration baroreflex test, various pathophysiological characteristics may be gained simultaneously.

The first purpose of this study was to examine whether a proposed wavelet-based time-frequency analysis was able to identify the dynamic as well as static baroreflex properties in animals from transient step pressure inputs with background noise during a short-duration test. Next, the proposed analysis was applied to identify unknown dynamic baroreflex properties in nonlinear AP input ranges during the Bezold-Jarisch reflex (BJR). We hypothesized that the proposed analysis could evaluate the baroreflex transfer properties from a short-term protocol, simultaneously at various pressure inputs under normal and BJR conditions. Finally, we examined the possibility of applying the new analysis to human studies to evaluate the dynamic baroreflex for AP regulation through the sympathovagal activity.

METHODS

Pathways of Baroreflex Functions

Under the carotid sinus open-loop condition, we defined the total loop as the system from carotid sinus pressure (CSP) input to AP output, which is divided into the neural arc as the subsystem from CSP input to renal sympathetic nerve activities (RSNA) output and the peripheral arc as the subsystem from RSNA input to AP output.[15] The cardiac baroreflex was defined as the system from CSP to heart rate (HR) response,[52] which may represent sympathovagal control of the heart through the baroreflex.

Surgical Preparations

Animals were cared for in accordance with the *Guiding Principles for the Care and Use of Animals in the Field of Physiological Sciences* approved by the Physiological Society of Japan. Japanese white rabbits were anesthetized with an intravenous injection (2 mL/kg) of a mixture of urethane (250 mg/mL) and α-chloralose (40 mg/mL) followed by a continuous administration (0.2–0.3 mL/kg/h, i.v.). The rabbits were artificially ventilated with oxygen-enriched room air at 0.6 Hz. Raw wave of AP was measured from the right femoral artery, using a high-fidelity pressure transducer (Millar Instruments, Houston, TX). A double-lumen catheter was placed into the right femoral vein for drug administration. The aortic depressor nerves identified by arterial pulse-synchronous activities were sectioned, while bilateral vagi were kept intact. Bilateral carotid sinuses were isolated from the systemic circulation by ligating the external and internal carotid arteries, and were filled with warm physiological saline through catheters inserted into the common carotid arteries. CSP was adjusted with a servo-controlled piston pump controlled by a computer system.

The left renal sympathetic nerve was exposed and a pair of stainless steel wire electrodes (Bioflex wire AS633, Cooner Wire) was attached. The nerve fibers distal to the electrodes were crushed by tight ligature to eliminate afferent signals from the kidney, and were covered in silicone gel (Semicosil 932A/B, Wacker Silicones). The preamplified nerve signal, band-pass filtered at 150–1000 Hz, was full-wave rectified and low-pass filtered at a cutoff frequency of 30 Hz (i.e. Op-amp RC integrator) to quantify nerve activity. Pancuronium bromide (0.3 mg/kg, i.v.) was administered to prevent muscular activity. The body temperature was kept at 38 °C.

Step Input Protocol

The carotid sinus baroreflex negative feedback loop was closed by adjusting CSP to AP level for 20 min after the surgical preparations (8 rabbits weighing 2.7–3.0 kg). The feedback loop was then opened and CSP was maintained at 40 mmHg for 4 min until the AP response reached a steady state. CSP was then increased from 40 to 160 mmHg in increments of 20 mmHg every minute (CSP_{40-60}, CSP_{60-80}, CSP_{80-100}, $CSP_{100-120}$, $CSP_{120-140}$, and $CSP_{140-160}$ changes). The single trial was repeated three times every rabbit. Data were sampled at 200 Hz and were averaged every 40 points for analysis (i.e. pulsatile AP signals were averaged every 0.2 s). HR (beats/min) was counted from the pulse waves of raw AP signals, which are well known as waves synchronized with ECG.[33] RSNA data of each animal were presented in arbitrary units (a.u.), with 1-min averaged background noise taken as zero level and 10-s averaged RSNA at CSP of 40 mmHg in normal condition set as unity.

Data Analysis

Identification of Dynamic Baroreflex

After the recorded data (three times) of CSP, RSNA, AP and HR were averaged in each animal, the signals were convoluted by complex Morlet wavelet, $w(t, f_0)$:[48,49]

$$w(t, f_0) = \frac{1}{\sqrt{\sigma_t\sqrt{\pi}}} \cdot \exp\left(\frac{-t^2}{2\sigma_t^2}\right) \cdot \exp(2\pi f_0 it) \qquad (1)$$

where the $(\sigma_t\sqrt{\pi})^{-1/2}$ normalizes the wavelets to be unity total energy, and the $\exp(-t^2/2\sigma_t^2)$ is a Gaussian shape with the central frequency f_0 at time t. The standard deviation (σ_t) of the time domain is inversely proportional to the standard deviation (σ_f) of the frequency domain [$\sigma_f = (2\pi\sigma_t)^{-1}$]. A constant ratio, f_0/σ_f, determines the effective number of oscillation cycles in the wavelet. The f_0/σ_f was determined[11] as 5 with f_0 ranging from 0.04 to 0.4 Hz[32] in increments of 0.01 Hz. Because the dynamic baroreflex function was well characterized by the transfer function up to around 0.4 Hz based on the corner frequency and slope of gain change,[15,32] the upper frequency limit for analysis was set at 0.4 Hz, considering also the limitation of the step input (low power in high frequency components) and the respiratory frequency of 0.6 Hz. The wavelet duration ($2\sigma_t$) is 39.8 s at 0.04 Hz and 3.98 s at 0.4 Hz, and the spectral band width ($2\sigma_f$) is 0.016 Hz at 0.04 Hz and 0.16 Hz at 0.4 Hz.

The linear trend was subtracted only in animal study, and the continuous wavelet transform of time series $u(t)$ was calculated as the convolution of a complex wavelet [$w(t, f_0)$] with the $u(t)$:

$$\tilde{u}(t, f_0) = w(t, f_0) * u(t) \qquad (2)$$

The power $P(t, f_0)$ of the signal in a frequency band at around f_0 is the squared norm of the wavelet transform: $P(t, f_0) = |\tilde{u}(t, f_0)|^2$. The symbol (*) shows the convolution in the time domain

To identify the dynamic baroreflex property from time-sequential data, we define the transfer function [$H(t, f_0)$] from input to output using wavelet transform as follows.

$$H(t, f_0) = \frac{P_{xy}(t, f_0)}{P_{xx}(t_{\text{event}}, f_0)} \qquad (3)$$

where

$$\begin{cases} P_{xx}(t_{\text{event}}, f_0) = \tilde{x}(t_{\text{event}}, f_0) \cdot \tilde{x}^{\oplus}(t_{\text{event}}, f_0) \\ P_{xy}(t, f_0) = \tilde{x}(t_{\text{event}}, f_0) \cdot \tilde{y}^{\oplus}(t, f_0) \end{cases}$$

$P_{xx}(t_{\text{event}}, f_0)$ is the auto-wavelet spectrum of the input signal [$x(t)$] with central frequency f_0 at a fixed time t_{event} when the power is maximum. The t_{event} shows the sole value of the analysis time (t) at f_0; the transfer function shows the effect of the maximum input power at t_{event} on the output responses during analysis time, t, for every f_0. Here, we used the fixed input value to extract the dynamics strictly against the step input. The cross-wavelet spectrum, $P_{xy}(t, f_0)$, which is an effective way to detect large-amplitude time-localized events,[26] is the convolution of the wavelet transform values of the input-output signals [$\tilde{x}(t_{\text{event}}, f_0)$ and $\tilde{y}^{\oplus}(t, f_0)$]. $\tilde{x}^{\oplus}(t_{\text{event}}, f_0)$ and $\tilde{y}^{\oplus}(t, f_0)$ is the complex conjugate of $x(t_{\text{event}}, f_0)$ and $y(t, f_0)$. The segment for wavelet transform analysis was set at ±30 s of the time of the step input change and was moved to the next area of the step input. The symbol (·) shows the product in the frequency domain, which corresponds to the convolution in the time domain.

To visualize the time-series transfer function during the analysis time (t), the dynamic gain $[|H(t, f_0)| = \sqrt{H_{\text{Re}}(t, f_0)^2 + H_{\text{Im}}(t, f_0)^2}$, where $H_{\text{Re}}(t, f_0)$ and $H_{\text{Im}}(t, f_0)$ are the real and imaginary parts of $H(t, f_0)$] and phase $\left[\varphi(t, f_0) = \tan^{-1}\frac{H_{\text{Im}}(t, f_0)}{H_{\text{Re}}(t, f_0)}\right]$ of the transient transfer function during analysis time were calculated from Eq. (3).

Next, we constructed the bode plot using the maximum dynamic gains, which reflects the maximum values of input and output powers. The phase of Eq. (3) is based on the maximum $P_{xx}(t_{\text{event}}, f_0)$ as the auto-wavelet spectrum of the input signal without the lag time of system response. To calculate the phase of the bode plot, we estimated the lag time of the system response as follows:

$$\hat{L} = t_{Pxy\max} - t_{Pxx\max}, \qquad (4)$$

where $\hat{L}$ is the mean value between 0.35 and 0.4 Hz of f_0. The data between 0.35 and 0.4 Hz (5 points) were averaged because of the varied estimation. The analysis time was set to 0–6 s and the phase unwrap process to make it continuous across 2π phase discontinuities by adding multiples of $\pm 2\pi$ was applied. $t_{Pxx\max}$ is the time at the maximum auto power spectrum of the input data; $t_{Pxy\max}$ is the time at the maximum cross power spectrum of input-output data. Using the estimated lag time (L) of the system response, the phase [$\varphi(t_{\max}, f_0)$] of the transient transfer function is shown as follows:

$$\varphi(t_{\max}, f_0) = \tan^{-1}\frac{H'_{\text{Im}}(t_{\max}, f_0)}{H'_{\text{Re}}(t_{\max}, f_0)} \qquad (5)$$

where

$$H'(t_{\max}, f_0) = H(t_{\max}, f_0) \cdot \exp(-2\pi f_0 iL)$$

$H'_{Re}(t_{max}, f_0)$ and $H'_{Im}(t_{max}, f_0)$ are the real and imaginary parts of $H'(t_{max}, f_0)$ with lag time, L. t_{max} is the time when the dynamic gain is maximum.

Static Characteristics

After the RSNA, AP, and HR during the last 10 s of each CSP level were averaged using the data of the step-input protocol, the static characteristics of total baroreflex loop, neural arc, and cardiac baroreflex control were examined by regression analysis for the logistic function.[24,46,47] To quantify static characteristics of the peripheral arc, linear regression analysis was performed. The closed-loop operating point of the baroreflex (AP_{OP}) was determined from the intersection point between the CSP-AP curve (total baroreflex loop) and CSP-AP identity line. AP_{OP} was also determined from AP at the intersection point between the CSP-RSNA curve (neural arc) and RSNA-AP line (peripheral arc) in the equilibrium diagram.[18]

Standard Analysis

The STFFT as a traditional time-frequency method was applied to the step-input (±20 mmHg) protocol, using the model response between CSP and AP (see Appendix). The time window was set to 12.8 s (64 data points) and 51.2 s (256 points, which is close to that at the lowest frequency in the used wavelet method). After the application of the detrend and Hanning window, power spectral densities of the CSP and AP and the transfer gain of the cross-spectra were computed every 200 ms. In the STFFT (256 points), pseudo-random noises were added to the input (within ±0.1 mmHg) and output (±1 mmHg every 200 ms) signals. The STFFT analysis was also compared with the proposed wavelet analysis over frequencies under the pseudo-random noise within ±0.1 mmHg in the input and ±1 or ±2 mmHg in output every 200 ms.

Experiment of Bezold-Jarisch Reflex

To elucidate the modified wavelet-based analysis in the pathophysiological condition, the previous datasets assessing static baroreflex during BJR[18] were reanalyzed; the data at sampling rate of 200 Hz were averaged every 40 points. In 8 anesthetized rabbits with sectioned aortic depressor nerves, intact vagi, and isolated carotid sinuses, CSP was increased stepwise while AP and HR were recorded before and after 7-min administration of a serotonin ($5\text{-}HT_3$) receptor agonist, phenylbiguanide (PBG, 100 μg/kg/min, intravenous infusion): Control and PBG conditions. Vagal afferent was confirmed as the main pathway of the BJR induced by intravenous PBG infusion.[20]

Cardiac Baroreflex

The role of cardiac baroreflex (CSP to HR response) was studied, focusing on the contribution of the cardiac sympathovagal activity to dynamic baroreflex for AP regulation. The ratio of the transfer functions between cardiac baroreflex and total (CSP-AP) loop was calculated under Control and PBG conditions, using the results from the proposed analysis.

Statistical Analysis

All data are expressed as mean ± SEM. The gain, power, and frequency in the figures are shown in log scales. The transfer functions in the neural and peripheral arcs were normalized in each animal so that the average gain in all stepwise changes of normal condition became unity at 0.04 Hz. To test the difference among six stepwise changes or between the Control and PBG conditions, we obtained the gain at 0.04 ($G_{0.04}$), the average slope of the gains between 0.1 to 0.4 Hz (Slope), and the lag time in each animal. One-way analysis of variance with multiple comparisons using Bonferroni correction[9] was applied to assess the level differences. Differences were considered statistically significant at $p < 0.05$.

Simulation for Closed-Loop Baroreflex

The carotid sinus open-loop animal experiment should be linked to human closed-loop baroreflex to explore the possibility of applying the proposed analysis to clinical diagnosis. We performed a simulation study, using the emulated cardiac baroreflex model from observed AP input to observed HR output under the closed-loop AP response (see Appendix) to test the accuracy of the proposed wavelet-based analysis and to acquire the transfer functions of the cardiac baroreflex for use in human laboratory test.

RESULTS

Test of Wavelet Analysis

The proposed wavelet-based analysis was tested using the baroreflex model response between CSP and AP under carotid sinus open-loop condition (see Appendix). After the calculation of the wavelet power spectrum for the input and the input-output cross spectrum (Fig. 2a), the transfer function was acquired (Fig. 2b). The gains reached the maximum immediately after the step input at 60 s and the phase changed greatly when approaching the maximum gain. Bode plots were extracted from the maximum points of the time-course transfer function with and without

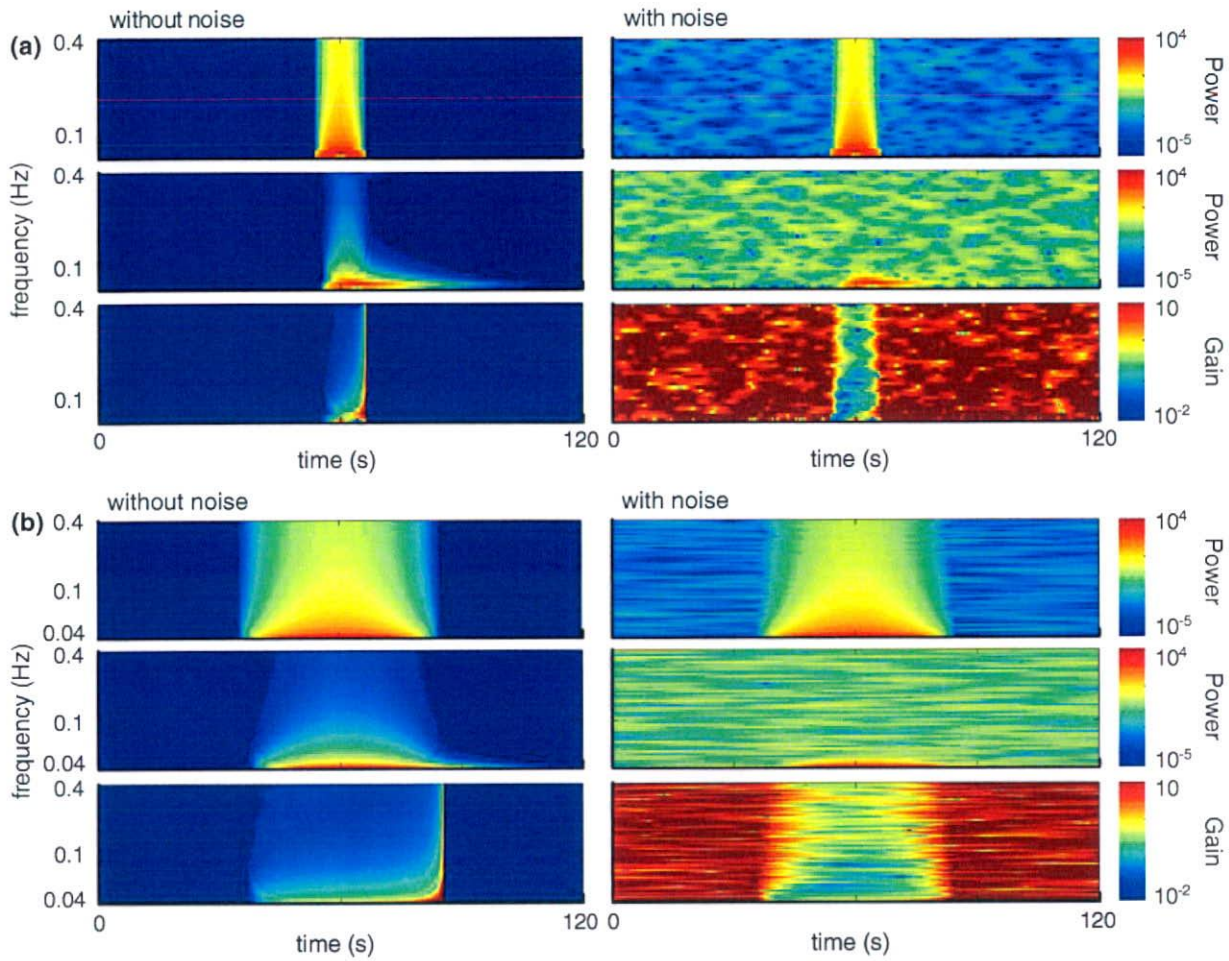

FIGURE 1. Time-frequency method based on the short-time FFT for system identification using the simulated step-input protocol. Time windows, 12.8 s (a) and 51.2 s (b). Power spectral densities of carotid sinus pressure (CSP) input (*top*) and arterial pressure (AP) output (*middle*) and transfer gain (*bottom*) in the absence (*left*) or presence (*right*) of pseudo-random noises.

background noise (Fig. 2c). In the presence of pseudo-random noise (within ±0.01 mmHg in input and ±1 mmHg in output changed every 200 ms), the transfer function closely resembled the theoretical values. Compared to the STFFT (Fig. 1), the proposed wavelet method could accurately estimate the transfer function over different frequencies, regardless of a poor signal to noise (S/N) ratio at higher frequency, because of the property of the step input power (Fig. 2d).

Dynamic Baroreflex

The averaged RSNA, AP, and HR responses to the step-input changes were decreased with the increments in CSP from 40 to 160 mmHg every minute ($n = 8$, Fig. 3a). In the averaged time series ($n = 8$, Fig. 3b), the power spectrums at all step inputs were the same values at each frequency level because of a constant change of +20 mmHg (greater in low frequency and smaller in high frequency). The powers of RSNA, AP, and HR change were higher at CSP_{80-100} than other CSP changes over all frequency ranges, and the magnitudes were especially small at low or high CSP changes.

The averaged ($n = 8$) time series of transfer functions in the neural arc (a), peripheral arc (b), total loop (c) and cardiac baroreflex (d) were calculated after wavelet transform (Fig. 4). In the neural arc, gain values in low frequencies were much less at CSP changes away from the operating point. In the peripheral arc, low pass characteristics in the gains were observed at all CSP changes except the lowest CSP_{40-60} change reflecting spontaneous neural firing. In the total baroreflex loop, the gains at CSP changes within 60–120 mmHg were higher than those at other CSP changes, indicating low-pass characteristics. In the cardiac baroreflex, the gains were smaller at the

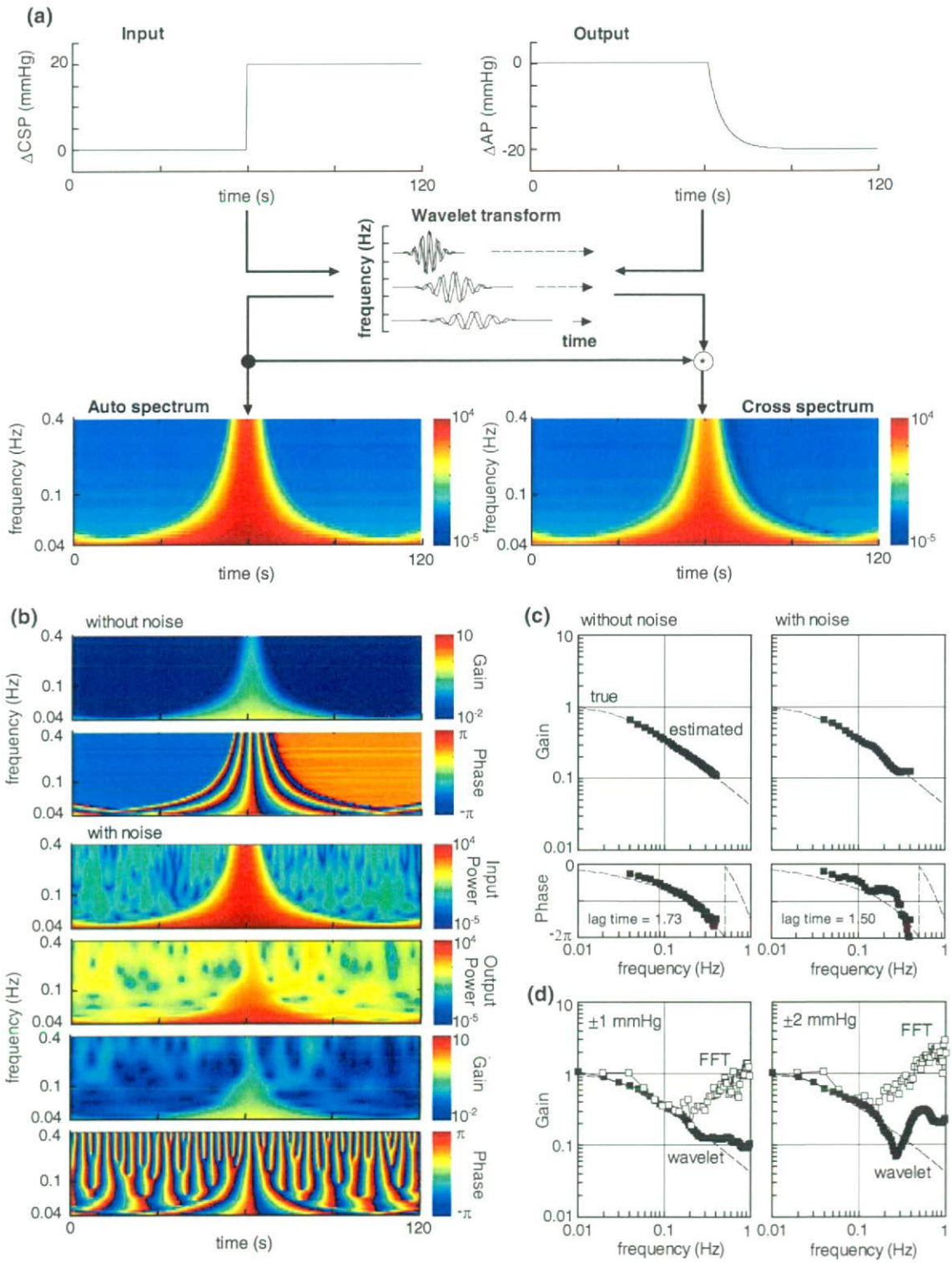

FIGURE 2. (a) Schematic illustration of the time-course system identification using wavelet analysis. The model response of total loop from CSP to AP under the carotid sinus open-loop condition was assessed for 120 s. Step input change of 20 mmHg was added to the system at 60 s. The time-series transfer function estimated by our wavelet analysis (b) and transfer function extracted from the time-course data of the total loop transfer function and the theoretical data (c). Gain (*top*) and phase (*bottom*) in the absence or presence of pseudo-random noise. (d) Gains in the short-time FFT and proposed wavelet analyses over wide frequencies (0.01–1 Hz) under the pseudo-random noise [±1 mmHg (*left*) and ±2 mmHg (*right*)].

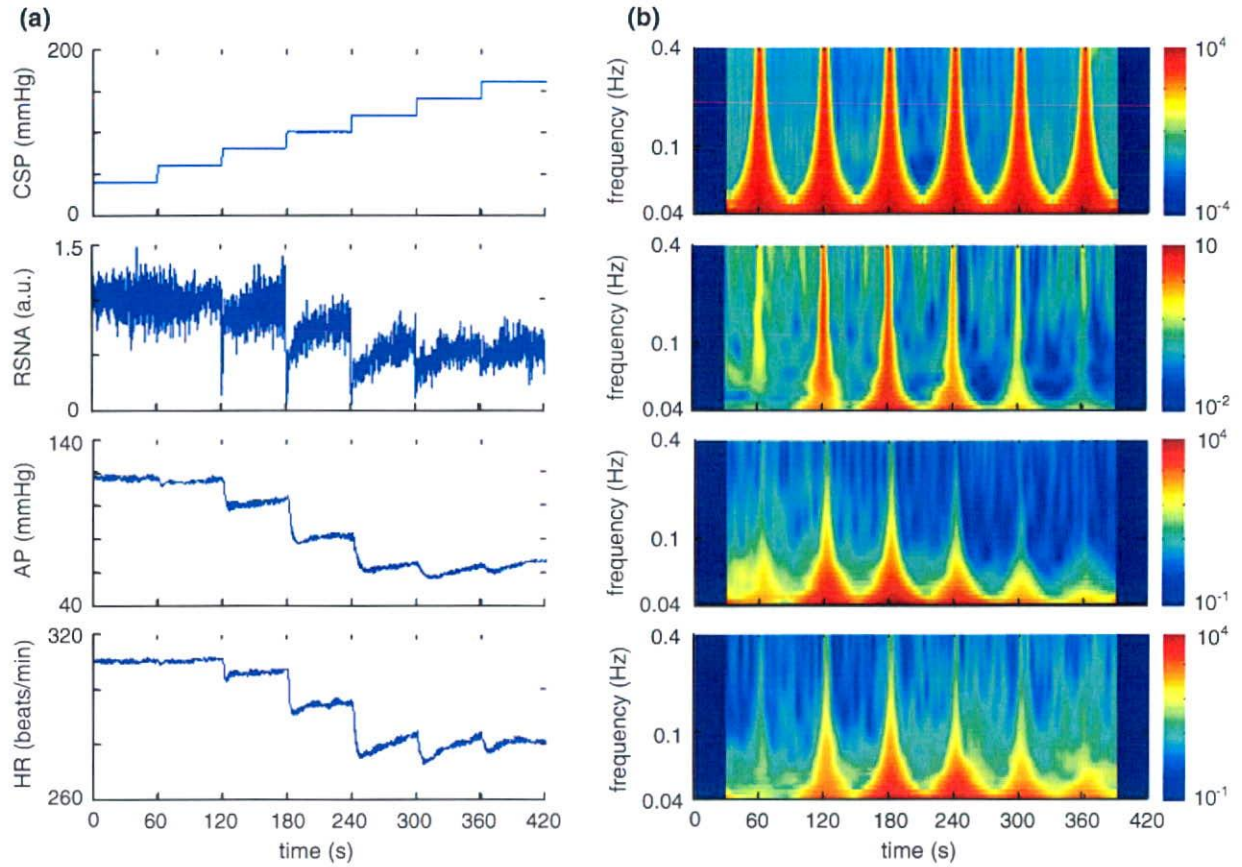

FIGURE 3. Averaged time series (a, $n = 8$) and wavelet power (b, $n = 8$) of CSP, renal sympathetic nerve activities (RSNA), AP, and heart rate (HR) during the static protocol. CSP was increased from 40 to 160 mmHg in 20 mmHg increments, resulting in changes of RSNA, AP, and HR through the carotid sinus baroreflex.

CSP_{40-60} and $CSP_{140-160}$ changes than other CSP changes.

Figure 5 and Table 1 show the average gain and phase ($n = 8$) in the neural arc (a), peripheral arc (b), total loop (c), and cardiac baroreflex (d). In the neural arc, $G_{0.04}$ (2.42 ± 0.07 a.u./mmHg) at the CSP_{80-100} change was the highest among all CSP changes, and was almost four to five times higher than those at the CSP_{40-60} (0.54 ± 0.09, $p < 0.01$) and $CSP_{140-160}$ (0.62 ± 0.06, $p < 0.01$) changes. Slopes increased significantly at lower and higher CSP changes compared with the $CSP_{100-120}$ change. Lag time at CSP_{80-100} was the shortest among all CSP changes. In the peripheral arc, Slope and lag time did not differ significantly among the CSP changes, whereas $G_{0.04}$ showed a tendency to decrease slightly with increase of CSP. In the total baroreflex, $G_{0.04}$ at CSP_{80-100} change (1.28 ± 0.12) was significantly higher compared to other CSP changes. Slopes were significantly greater at CSP changes within 60–120 mmHg than other CSP changes. Lag time did not differ significantly among CSP changes. In the cardiac baroreflex, $G_{0.04}$ (0.90 ± 0.18 and 0.92 ± 0.19 beats/min/mmHg) and Slopes were significantly higher at CSP_{80-100} and $CSP_{100-120}$ changes than other CSP changes. There were no significant differences in lag time among CSP changes.

Static Baroreflex

The static characteristics of the total loop were averaged ($n = 8$). Regression analysis was performed for logistic functions. Response range, coefficient of gain, midpoint of input axis, and minimum value of output were 0.45, 0.11, 99.6, and 0.55 in the neural arc, 65.2, 0.07, 97.6, and 69.4 in the total loop, and 29.5, 0.11, 98.2, and 281.2 in the cardiac baroreflex. Linear regression analysis was performed in the peripheral arc (static gain = 0.0086 and offset pressure = 0.027). The intersection between the CSP-AP curve and the line of identity corresponds to AP_{OP} (94.3 mmHg) located in the steepest portion (80–100 mmHg) of the sigmoid

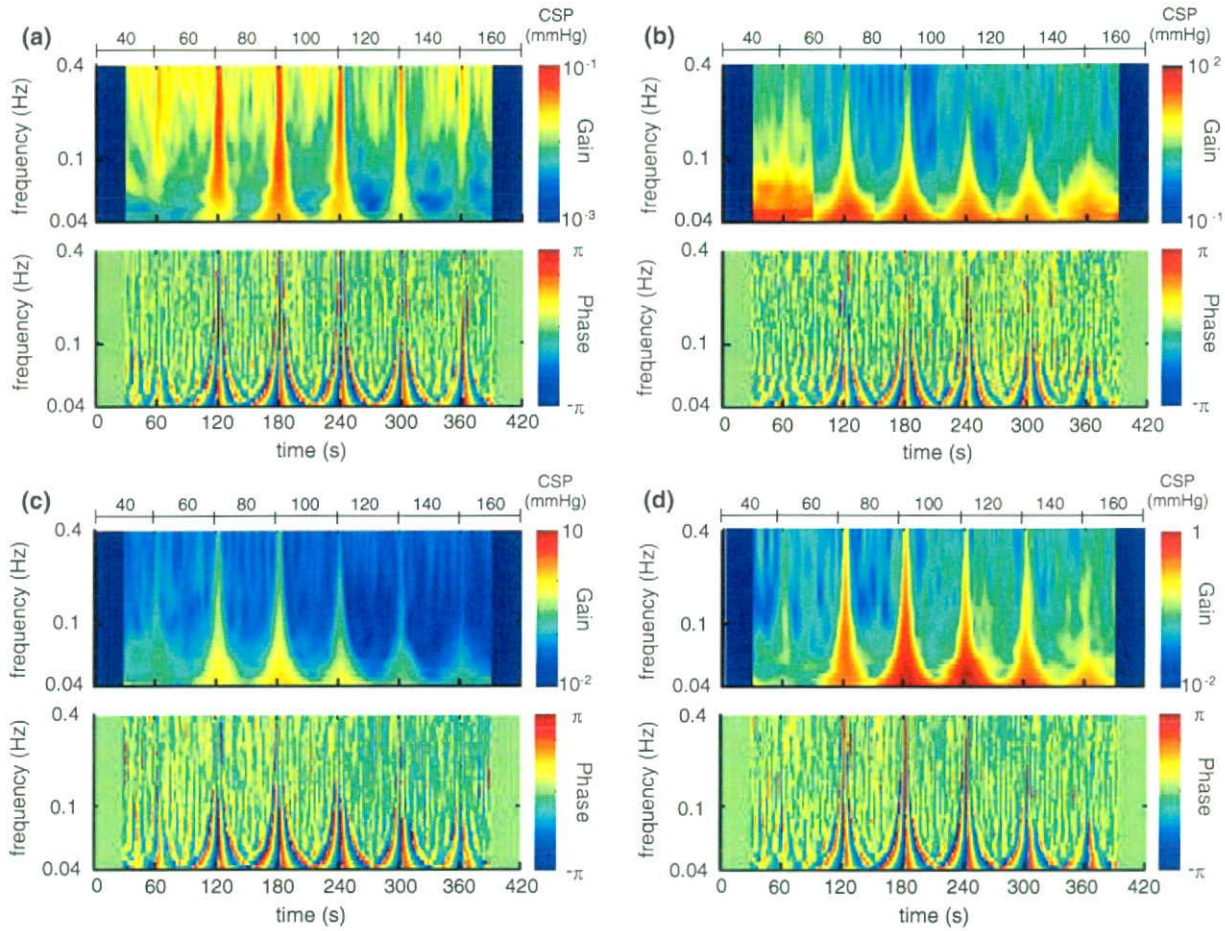

FIGURE 4. Time course of transfer functions of the neural arc from CSP to RSNA (a), peripheral arc from RSNA to AP (b), total baroreflex loop from CSP to AP (c), and cardiac baroreflex from CSP to HR (d) averaged across all animals (n = 8).

curve. In the equilibrium diagram, RSNA decreased with increasing CSP in the neural arc, AP increased with increasing RSNA in the peripheral arc, and the intersection between the two arcs provided the AP_{OP} (99.7 mmHg). In the cardiac baroreflex, HR decreased with the increase in CSP.

Bezold-Jarisch Reflex

In the total loop and cardiac baroreflex, the gains at various CSP changes during the BJR were identified ($n = 8$, Fig. 6 and Table 2). Averages of gain and phase (Fig. 6d) were derived from the time series in Figs. 6b and 6c. At middle CSP change of the total loop, $G_{0.04}$ was approximately halved under PBG condition compared to Control (0.59 ± 0.09 vs. 1.39 ± 0.15, $p < 0.01$). Slope and lag time did not differ significantly between the PBG and Control conditions at all CSP changes. In the cardiac baroreflex (Fig. 6e), $G_{0.04}$ tended to modulate under PBG condition at low and high CSP changes, but did not differ significantly between the two conditions at middle CSP changes. Slope differed significantly between the two conditions at low CSP change whereas lag time did not differ significantly at all CSP changes.

Cardiac Baroreflex

The ratio of the cardiac baroreflex to the total loop in dynamic characteristics was studied (Fig. 7). For CSP changes within 60–120 mmHg under Control condition, the ratios were almost linear and increased slightly with increase in frequency; in lower or higher CSP changes, they were modulated especially around 0.2 Hz. For CSP changes under PBG condition, overall the ratios were higher than those under Control condition. For CSP changes within 80–120 mmHg under PBG condition, the ratios were almost linear and the slopes were greater than those of Control condition; in lower or higher CSP changes, they

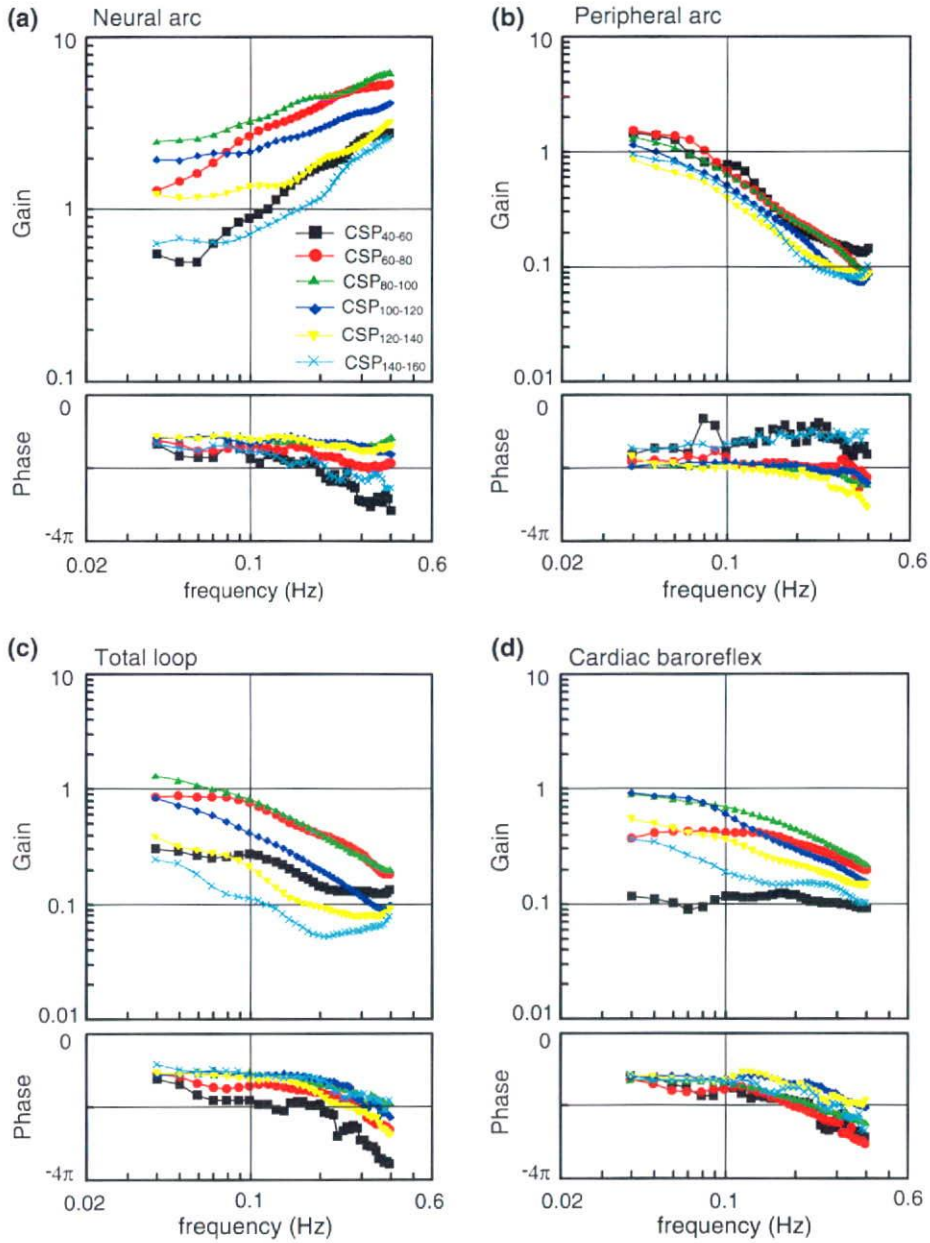

FIGURE 5. Transfer functions of the neural arc from CSP to RSNA, effective peripheral arc from RSNA to AP, total baroreflex loop from CSP to AP, and cardiac baroreflex estimated by wavelet analysis. Average (n = 8) gain (*top*) and phase (*bottom*).

increased within the 0.1–0.2 Hz range and decreased at higher frequencies. The phase difference did not differ among CSP changes under both Control and PBG conditions.

Closed-Loop Baroreflex

Simulation was performed using a cardiac baroreflex system from closed-loop AP input to HR output (Fig. 8a). To test the proposed wavelet analysis, an external disturbance to AP (AP_{noise} = +20 mmHg) was added to the system, and HR responses under carotid sinus open- and closed-loop AP responses were calculated (Fig. 8b). The observed AP and HR (AP_{change} and HR_{change}) were modulated by closed-loop regulation of AP. The CSP is identical with the observed AP_{change}. Gain and phase in the time series (Fig. 8c) and extracted (Fig. 8d) transfer functions were accurately estimated under open and closed AP responses.

TABLE 1. Parameters of the transfer functions in the neural arc, peripheral arc, total loop, and cardiac baroreflex at various step pressure inputs.

	CSP (mmHg)					
	40–60	60–80	80–100	100–120	120–140	140–160
Neural arc						
$G_{0.04}$ (a.u./mmHg)	0.54 ± 0.09	1.25 ± 0.17**	2.42 ± 0.07**,††	1.89 ± 0.13**,†	1.18 ± 0.20**,‡‡,¶¶	0.62 ± 0.06†,‡‡,¶¶
Slope (dB/decade)	17.9 ± 4.1	10.0 ± 1.9	7.7 ± 2.0	5.8 ± 3.1*	11.0 ± 1.8	16.8 ± 3.1¶
Lag time (s)	2.63 ± 0.58	0.78 ± 0.16*	0.27 ± 0.18**	0.48 ± 0.14**	0.45 ± 0.17**	1.83 ± 0.71
Peripheral arc						
$G_{0.04}$ (mmHg/a.u.)	1.42 ± 0.17	1.50 ± 0.18	1.30 ± 0.08	1.13 ± 0.13	0.85 ± 0.10†	0.92 ± 0.09†
Slope (dB/decade)	−24.6 ± 3.3	−29.4 ± 1.3	−28.2 ± 0.8	−26.6 ± 2.8	−22.7 ± 2.8	−23.2 ± 4.6
Lag time (s)	0.40 ± 0.79	1.29 ± 0.20	1.35 ± 0.20	1.35 ± 0.58	2.10 ± 0.69	0.08 ± 0.64
Total loop						
$G_{0.04}$	0.29 ± 0.05	0.85 ± 0.16**	1.28 ± 0.12**,††	0.83 ± 0.09**,‡‡	0.38 ± 0.07††,‡‡,¶¶	0.24 ± 0.04††,‡‡,¶¶
Slope (dB/decade)	−6.8 ± 4.1	−19.4 ± 2.4**	−20.5 ± 1.6**	−20.7 ± 2.1**	−11.8 ± 2.7	−6.4 ± 4.1††,‡‡,¶¶
Lag time (s)	3.03 ± 0.61	2.07 ± 0.12	1.62 ± 0.20	1.82 ± 0.60	2.54 ± 0.62	1.91 ± 0.41
Cardiac baroreflex						
$G_{0.04}$ (beats/min/mmHg)	0.11 ± 0.02	0.37 ± 0.11	0.90 ± 0.18**,††	0.92 ± 0.19**,††	0.55 ± 0.12**,‡,¶	0.36 ± 0.09‡‡,¶¶
Slope (dB/decade)	−2.3 ± 2.1	−10.7 ± 2.3	−15.9 ± 2.8**	−19.0 ± 2.9**	−11.8 ± 2.6	−6.3 ± 3.1‡,¶¶
Lag time (s)	2.13 ± 0.62	2.26 ± 0.34	2.17 ± 0.62	1.51 ± 0.16	1.70 ± 0.61	1.92 ± 0.86

$G_{0.04}$, transfer gain at 0.04 Hz. Slope, average slope of transfer gain between 0.1 and 0.4 Hz.
$p < 0.01$; ** vs. 40–60, †† vs. 60–80, ‡‡ vs. 80–100, and ¶¶ vs. 100–120 mmHg in CSP change; the same symbols of a single show $p < 0.05$.

DISCUSSION

We have shown that the analysis using wavelet transform can identify the dynamic baroreflex properties at various pressure levels from the time-course data under normal (Fig. 5) and pathophysiological conditions (Fig. 6) with background noise. The results of the proposed analysis applied in animal experiments indicate the possibility of its use in the assessment of human baroreflex (Figs. 7 and 8).

Time-Series Analysis for Dynamic Baroreflex

Under the background noise added to the response model, the proposed analysis applied to step response was able to detect the dynamic baroreflex characteristics (Fig. 2). The standard spectral analysis under stationary conditions has high reliability in the baroreflex test, and uses longer data to cancel the noise[31,38] at various pressure inputs and lose the short-term and important changes. In direct calculation of the dynamic characteristics from the step input output data, the traditional time series analysis might also have a disadvantage under noise contamination, which may cause poor S/N ratio in the impaired baroreflex function of cardiac diseases.[41] The STFFT using time windows of a constant range for all frequencies was actually unable to catch the dynamic property especially at higher frequencies under such condition (Figs. 1 and 2d) because of the average one within the whole time window. On the other hand, the modified wavelet-based analysis with improved temporal resolution at higher frequencies to reasonably catch the localized changes in cardiovascular control[4,50] will be effective for extracting the dynamic baroreflex characteristics under nonstationary hemodynamics with a low S/N ratio. Because the baroreflex test may depend on the various S/N ratios depending on the system input (e.g. amplitude) and/or the background noises, further investigations will be required in this regard.

Burgess *et al.*[2] showed that cross spectrum analysis using wavelet transform characterized strong coupling between sympathetic nerve traffic and AP at frequencies of <0.1 Hz. Davrath *et al.*[4] reported that time-varying power obtained from wavelet transform of the spontaneous HR or AP fluctuation in humans are remarkably modulated at approximately 0.1 Hz under standing condition. Whereas the traditional wavelet analysis could extract the localized characteristics of time-series data in a nonstationary condition,[2,4] application to dynamic system identification is difficult because of the limitation in phase extraction. When the same time window is set for the input and output data, the actual information of phase and gain may be lost or split, instead of high temporal resolution of wavelet transform.[34] To apply wavelet analysis to the baroreflex system identification, we expanded the basic analysis by acquiring the transfer function from maximum input and output data. The proposed method was able to acquire the system identification of baroreflex because of the specific characteristics of wavelet

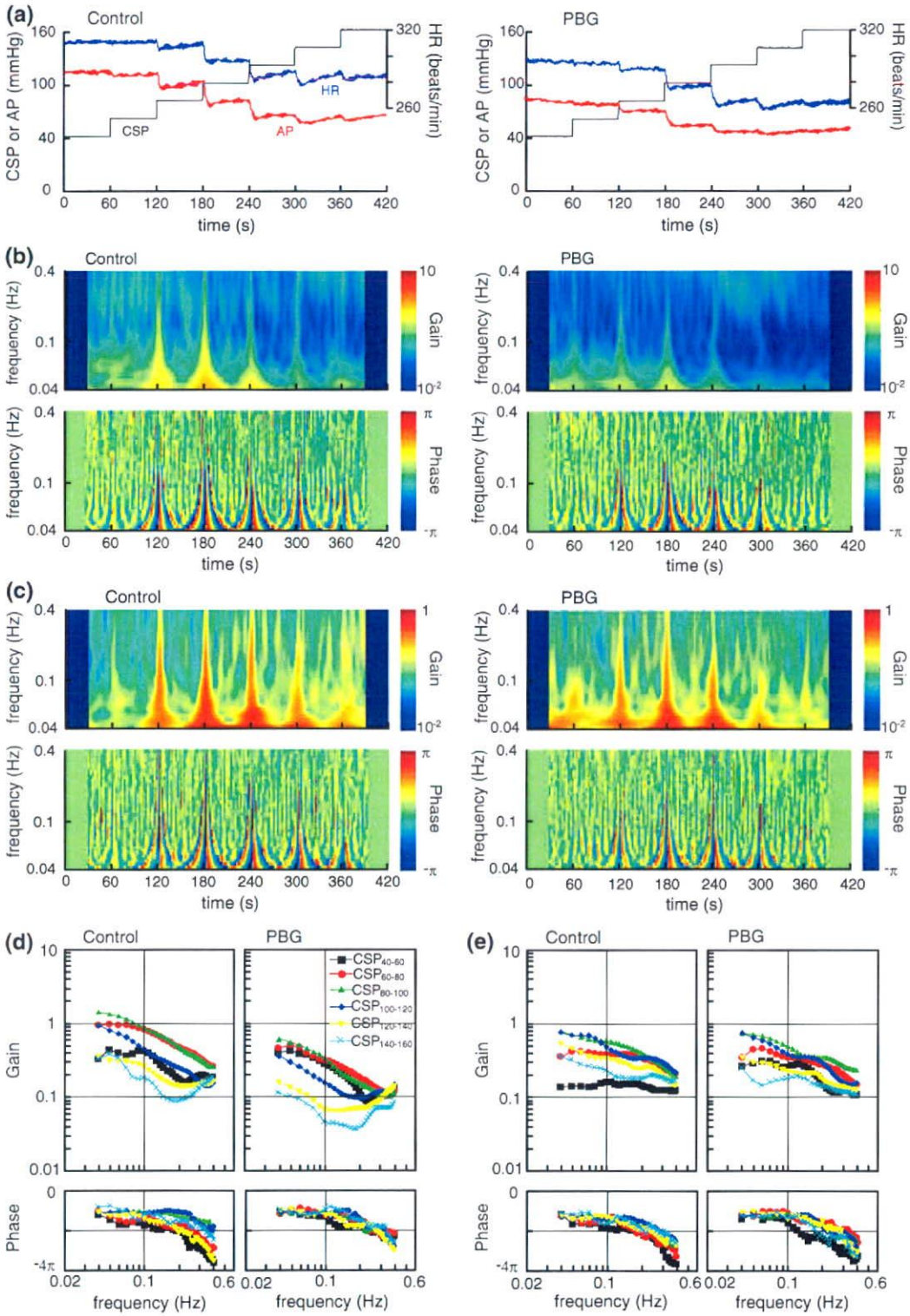

FIGURE 6. (a) Averaged (n = 8) time series of CSP, AP, and HR obtained in the absence (Control, *left*) and presence of phenylbiguanide (PBG, *right*). CSP was increased from 40 to 160 mmHg in 20 mmHg increments, resulting in changes in AP and **HR through the carotid sinus baroreflex. Time-series transfer functions of total loop (b) and cardiac baroreflex (c) in the Control** (*left*) and PBG (*right*) conditions. Average (n = 8) gain (*top*) and phase (*bottom*). Transfer functions of total loop (d) and cardiac **baroreflex (e) estimated by wavelet analysis in the Control (*left*)** and PBG (*right*) conditions.

TABLE 2. Parameters of the transfer functions for the total loop and cardiac baroreflex before and during PBG infusion.

	Low CSP (40–60 mmHg)		Middle CSP (80–100 mmHg)		High CSP (120–140 mmHg)	
	Control	PBG	Control	PBG	Control	PBG
Total loop						
$G_{0.04}$	0.32 ± 0.07	0.39 ± 0.09††	1.39 ± 0.15	0.59 ± 0.09**,††	0.35 ± 0.04††	0.15 ± 0.02††
Slope (dB/decade)	−11.6 ± 3.3	−8.0 ± 4.2	−17.8 ± 2.1	−15.0 ± 3.2	−6.5 ± 2.5	7.4 ± 5.3††
Lag time (s)	2.90 ± 0.71	1.43 ± 0.68	1.44 ± 0.22	2.21 ± 0.59	3.48 ± 0.61	2.74 ± 0.89
Cardiac baroreflex						
$G_{0.04}$ (beats/min/mmHg)	0.14 ± 0.02	0.26 ± 0.10†	0.78 ± 0.21	0.75 ± 0.18	0.54 ± 0.13	0.35 ± 0.08†
Slope (dB/decade)	−1.8 ± 2.2	−12.5 ± 2.9*	−13.4 ± 2.7	−11.6 ± 2.1	−12.6 ± 2.7	−6.6 ± 4.0
Lag time (s)	2.99 ± 0.89	2.91 ± 0.55	2.06 ± 0.30	2.28 ± 0.54	2.65 ± 0.72	2.47 ± 0.77

$G_{0.04}$, transfer gain at 0.04 Hz. Slope, average slope of gain between 0.1 and 0.4 Hz. PBG, phenylbiguanide.
** $p < 0.01$ and * $p < 0.05$, PBG vs. Control at the same CSP; †† $p < 0.01$ and † $p < 0.05$, all conditions vs. CSP_{80-100} of Control.

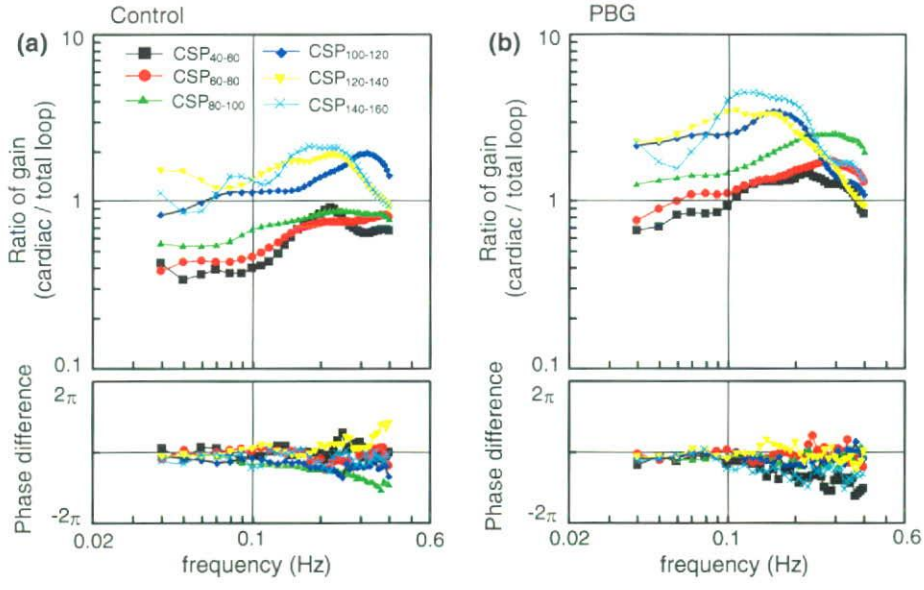

FIGURE 7. The ratio in the transfer functions of the cardiac baroreflex (CSP-HR) to the total loop (CSP-AP) (n = 8). The ratio of dynamic gain (*top*) and the phase difference (*bottom*). Control (a) and PBG (b) conditions.

transform that can adjust the analysis window at every frequency level and extract the localized data. When the mother wavelet is appropriately used for any purpose, the fields of the application of wavelet analysis might be extended. We used the traditional and reasonable Morlet function;[11,48,49] however, the comparison with other wavelet functions such as Mexican hat, Haar, and Daubechies[34] will be required in future studies. In addition, the convolutions within the transfer function of Eq. (3) may lose the temporal information; however, because the wavelet transform reflects the effect of reasonably changed time window, the gain and phase updated every 0.2 s can continuously express the representative property at the center point of the time window during the time-course change.

Physiological Perspective

The powers of the RSNA, AP, and HR responses to CSP changes showed maximum values at CSP_{80-100} change (Fig. 3b), which was almost consistent with AP_{OP} (94.3 and 99.7 mmHg) from static analysis. In contrast, the power responses at CSP_{40-60} and $CSP_{140-160}$ changes were lower than those at AP_{OP}, resulting from the nonlinear characteristics of the baroreflex around threshold and saturation to AP inputs as indicated by the static analysis. The gain and phase were revealed within the physiological range including nonlinear points in normal rabbits (Figs. 4 and 5). Whereas the static analysis cannot show the dynamic characteristics at higher frequencies (e.g. >0.01 Hz[18]), the proposed wavelet-based analysis

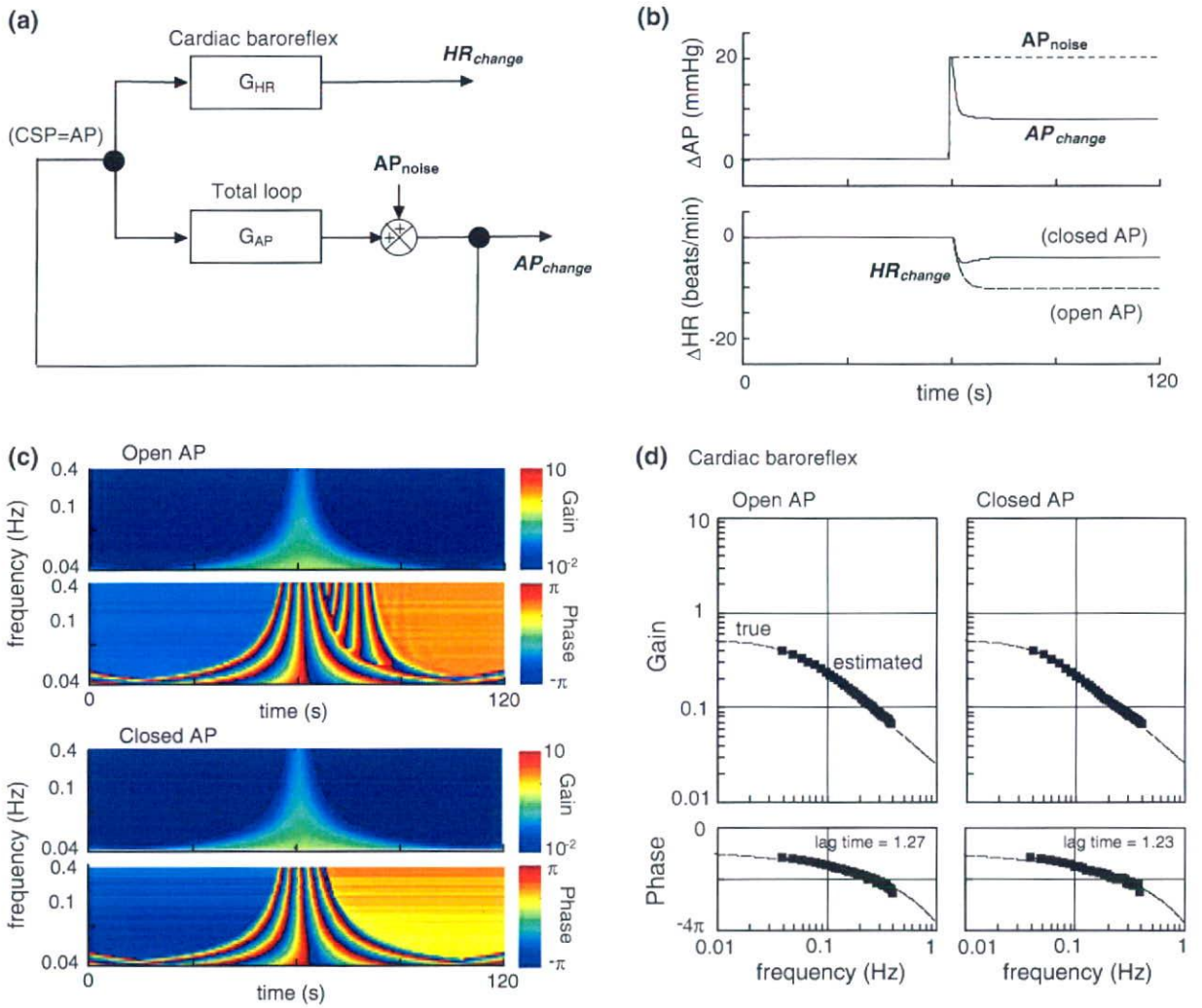

FIGURE 8. (a) Block diagram of cardiac baroreflex under closed-loop AP response. AP_{noise} indicates the external disturbance to AP. AP_{change} and HR_{change} show the actual changes of AP and HR. G_{AP} and G_{HR} are transfer functions under open loop responses in the total loop and cardiac baroreflex. (b) AP_{noise} of +20 mmHg as input and AP_{change} as output under the closed loop (*top*). HR responses under the open- and closed-loop AP changes (*bottom*). (c) Time-series transfer functions of cardiac baroreflex under open- and closed-loop AP changes. (d) Transfer functions of cardiac baroreflex estimated under the open (*left*) and closed (*right*) AP responses. Gain (*top*) and phase (*bottom*). Dotted lines, theoretical values. Squares, estimated values by our wavelet analysis.

could derive them from the same step input protocol, which may be able to reduce the number of experiments and duration of data acquisition.

Clinical Implications for Cardiac Patients

The wavelet-based system identification indicated a possibility to acquire pathophysiological understanding under various responses with cardiac diseases. The proposed analysis revealed that the dynamic characteristics in the total loop and neural arc were significantly attenuated at various pressure changes containing nonlinear points under PBG condition (Fig. 6 and Table 2), in addition to the previous studies.[18,20] The $G_{0.04}$ at AP_{OP} in Control (1.39 ± 0.15) was decreased to almost half during PBG condition (0.59 ± 0.09); it was attenuated to 1/3–1/4 times as small as that under PBG condition (0.39 ± 0.09) at low CSP_{40-60} change, which may be induced by the decrease of peripheral pump function in heart failure, suggesting the risk of further bluntness of baroreflex ability during the BJR.

In carotid-cardiac response, HR may be related to the assessment of AP regulation by the product of HR, stroke volume, and total peripheral resistance, rather than RR interval.[7,8] Because it may be difficult to evaluate the baroreflex to regulate AP under the carotid-sinus closed loop condition (i.e. CSP = AP), we

explored the possibility to evaluate the baroreflex dynamics from the HR response related to AP regulation, considering the dissociation between animal and human studies and applying the proposed method. The transfer functions of the cardiac baroreflex were similar to those of the total loop around the operating point (Fig. 7a). On the other hand, the dynamic characteristics in nonlinear CSP points and during the BJR were greater than those around the operating point in Control condition (Fig. 7b), suggesting the effect of cardiac sympathovagal activity. Next, to consider human baroreflex assessment, the dynamic transfer function was estimated by the closed-loop model response (Fig. 8), resulting in the effective assessment. Even when the system input is modulated by the nature of closed-loop response, it would be crucial to be able to estimate the dynamic baroreflex characteristics.

The spontaneous baroreflex method is commonly used in clinical assessments.[37] This method may have some limitations because of the highly complex and interconnected cardiovascular mechanisms in short-term AP regulation[27,40,43] and the unclear system input might induce the different pathophysiological understandings.[42] On the other hand, our focus was to explore the possibility of the evaluation of the baroreflex to regulate AP against great external disturbances in patients with cardiovascular diseases and unstable hemodynamics. To identify the system dynamics of the carotid-sinus baroreflex for AP regulation with sympathovagal activity,[51] this study improved the standard analyses, particularly considering the pure time delay. Using the transfer function corresponding to the independent step input frequency, the proposed analysis was able to indicate some novel aspects of the dynamic baroreflex properties during the BJR as mentioned above.

For clinical application, the other indexes (e.g. AP to muscle SNA response[14]) for AP regulation might be tested. In addition, in the time-course data, there are some effective methods such as complex demodulation method[13] based on the low pass filter, focusing on a frequency band such as LF and HF; it has good temporal resolution. However, the complex demodulation method might concentrate on the information of amplitude in a frequency band, not on each frequency level within the band. This limitation makes it impossible to perform the system identification in this study to reproduce the response corresponding to a wide frequency. Furthermore, the continuous estimation of the dynamics might connect to an effective index of the real-time control of hemodynamics such as an automated drug infusion system.[17,19]

Because we kept the bilateral vagi intact, low pressure baroreflexes from the cardiopulmonary region might have interacted with the arterial baroreflex, affecting estimation of carotid sinus baroreflex transfer functions. After the vagotomy, the dynamics from isolated aortic depressor nerve to AP responses was almost preserved and AP remained unchanged despite a HR decrease.[28,46] Our previous data of dynamic baroreflex properties with[20] and without[21] vagal nerves were compared. The dynamic characteristics of the total loop and cardiac baroreflex around the operating point were similar, whereas the corner frequency was slightly greater under intact vagal condition. Next, the static gain may be increased during the rising pressure protocol, compared with the falling one.[46] Hysteresis induced by the rising and falling pressure protocols may also modulate the dynamic baroreflex. However, the vagal effect of the cardiovascular receptors on the dynamics may not be large.[28] Third, the phases at lower or higher CSP changes in the transfer functions varied with the observed frequency because of nonlinear characteristics in the neural arc and the input power in the peripheral arc decreased by the neural arc. Especially at high frequencies, the phases appear to be modulated because of the step input showing low power with the high frequency. Finally, the simple models used for the simulations in this study have some limitations, such as a lack of information of nonparametric components or nonlinearity.[23]

CONCLUSIONS

The wavelet-based time-frequency analysis was capable of identifying the dynamic baroreflex properties over wide frequencies at various pressure levels both in normal and BJR conditions. Because the dynamic baroreflex properties to physiological pressure inputs as well as static characteristics can be simultaneously extracted from the short-term responses with background noise, the proposed method is potentially applicable to assess human dynamic baroreflex function under carotid-sinus closed-loop condition.

APPENDIX

Model Response of Arterial Baroreflex

We used the following model[15] as the carotid sinus open loop baroreflex for the simulation study (Figs. 1 and 2). The neural arc transfer function [$G_N(f)$] using a first-order high-pass filter can be expressed as

$$G_N(f) = -K_N\left(1 + \frac{f}{f_C}i\right)\exp(-2\pi f i L_N)$$

where f and i represent the frequency (Hz) and imaginary units, respectively; $K_{\mathbf{N}}$ is the neural arc gain; $f_{\mathbf{C}}$ is the frequency (Hz) for a derivative characteristic; $L_{\mathbf{N}}$ is lag time (s).

The peripheral arc transfer function [$G_{\mathbf{P}}(f)$] using a second-order low-pass filter can be expressed as

$$G_{\mathrm{P}}(f) = \frac{K_{\mathrm{P}}}{1 + 2\zeta\frac{f}{f_{\mathrm{N}}}i + \left(\frac{f}{f_{\mathrm{N}}}i\right)^2} \exp(-2\pi f i L_{\mathrm{P}})$$

where $K_{\mathbf{P}}$, $f_{\mathbf{N}}$, ζ, and $L_{\mathbf{P}}$ represent the peripheral arc gain, natural frequency (Hz), damping ratio, and lag time (s), respectively.

The transfer function of the total baroreflex loop is expressed as the product of the neural and peripheral arc transfer functions.

$$G_{\mathrm{AP}}(f) = G_{\mathrm{N}}(f) \cdot G_{\mathrm{P}}(f)$$

The gain and lag time of the total baroreflex loop is expressed as $K = K_{\mathbf{N}} \cdot K_{\mathbf{P}}$ and $L = L_{\mathbf{N}} + L_{\mathbf{P}}$. The parameters of the model response were set at $K = 1.0$, $f_{\mathbf{C}} = 0.12$, $L_{\mathbf{N}} = 0.55$, $f_{\mathbf{N}} = 0.071$, $\zeta = 1.37$, and $L_{\mathbf{P}} = 1.0$ according to previous data.[15]

Model of Baroreflex Under Closed-Loop AP Response

The baroreflex system under the closed-loop AP input to HR response was modeled (Fig. 8a).

$$\mathrm{HR}_{\mathrm{change}}(f) = G_{\mathrm{HR}}(f) \cdot \mathrm{AP}_{\mathrm{change}}(f)$$

The pressure change [$\mathrm{AP}_{\mathbf{change}}(f)$] to the exogenous perturbation [$\mathrm{AP}_{\mathbf{noise}}(f)$] is the sum of the feedback signal and perturbation under closed-loop condition.[15] $G_{\mathbf{HR}}$ is the transfer function under the carotid sinus open loop in the cardiac baroreflex (CSP input and HR output).

$$\mathrm{AP}_{\mathrm{change}}(f) = G_{\mathrm{AP}}(f) \cdot \mathrm{AP}_{\mathrm{change}}(f) + \mathrm{AP}_{\mathrm{noise}}(f)$$

Rearranging above equation with respect to $\mathrm{AP}_{\mathbf{change}}(f)$ yields

$$\mathrm{AP}_{\mathrm{change}}(f) = \frac{\mathrm{AP}_{\mathrm{noise}}(f)}{1 - G_{\mathrm{AP}}(f)}$$

The time integral of the inverse Fourier transform of $\mathrm{AP}_{\mathbf{change}}(f)$ is the AP change to an exogenous step perturbation. $G_{\mathbf{AP}}$ is the transfer function under the carotid sinus open loop for the total baroreflex. The $\mathrm{AP}_{\mathbf{change}}$ and $\mathrm{HR}_{\mathbf{change}}$ can be simply observed by the monitoring system. The transfer function between the HR and AP responses was excluded because of the insignificant relationship as previously indicated.[22]

The transfer functions, $G_{\mathbf{AP}}$ and $G_{\mathbf{HR}}$, were approximated using a first-order low-pass filter.

$$G(f) = \frac{-K}{\left(1 + \frac{f}{f_{\mathrm{C}}}i\right)} \cdot \exp(-2\pi f i L)$$

The parameters of the transfer functions were set at $K = 1.03$, $f_{\mathbf{C}} = 0.018$, and $L = 1.34$ for the total loop (Fig. 8a, $G_{\mathbf{AP}}$); $K = 0.51$, $f_{\mathbf{C}} = 0.049$, and $L = 1.14$ for the cardiac baroreflex ($G_{\mathbf{HR}}$), according to previous data.[20]

ACKNOWLEDGMENTS

This study was supported by "Health and Labour Sciences Research Grant for Research on Advanced Medical Technology", "Health and Labour Sciences Research Grant for Research on Medical Devices for Analyzing, Supporting and Substituting the Function of Human Body", "Health and Labour Sciences Research Grant H18-Iryo-Ippan-023" from the Ministry of Health, Labour and Welfare of Japan, "Program for Promotion of Fundamental Studies in Health Science" from the National Institute of Biomedical Innovation, and "a Grant-in-Aid for Young Scientists (B)" from the Ministry of Education, Culture, Sports, Science and Technology of Japan (KAKENHI, 20700392).

REFERENCES

[1]Ando, S., H. R. Dajani, B. L. Senn, G. E. Newton, and J. S. Floras. Sympathetic alternans. Evidence for arterial baroreflex control of muscle sympathetic nerve activity in congestive heart failure. *Circulation* 95:316–319, 1997.

[2]Burgess, D. E., D. C. Randall, R. O. Speakman, and D. R. Brown. Coupling of sympathetic nerve traffic and BP at very low frequencies is mediated by large-amplitude events. *Am. J. Physiol. Regul. Integr. Comp. Physiol.* 284:R802–R810, 2003.

[3]Dampney, R. A. Functional organization of central pathways regulating the cardiovascular system. *Physiol. Rev.* 74:323–364, 1994.

[4]Davrath, L. R., Y. Goren, I. Pinhas, E. Toledo, and S. Akselrod. Early autonomic malfunction in normotensive individuals with a genetic predisposition to essential hypertension. *Am. J. Physiol. Heart Circ. Physiol.* 285:H1697–H1704, 2003.

[5]Eckberg, D. L., and T. A. Kuusela. Human vagal baroreflex sensitivity fluctuates widely and rhythmically at very low frequencies. *J. Physiol.* 567:1011–1019, 2005. doi:10.1113/jphysiol.2005.091090.

[6]Ellenbogen, K. A., P. K. Mohanty, S. Szentpetery, and M. D. Thames. Arterial baroreflex abnormalities in heart failure: reversal after orthotopic cardiac transplantation. *Circulation* 79:51–58, 1989.

[7]Fadel, P. J., S. Ogoh, D. M. Keller, and P. B. Raven. Recent insights into carotid baroreflex function in humans

using the variable pressure neck chamber. *Exp. Physiol.* 88:671–680, 2003. doi:10.1113/eph8802650.

[8]Fadel, P. J., M. Stromstad, D. W. Wray, S. A. Smith, P. B. Raven, and N. H. Secher. New insights into differential baroreflex control of heart rate in humans. *Am. J. Physiol. Heart Circ. Physiol.* 284:H735–H743, 2003.

[9]Glantz, S. A. Primer of Biostatistics. 4th ed. New York: McGraw Hill, 1997.

[10]Grassi, G., C. Turri, G. Seravalle, G. Bertinieri, A. Pierini, and G. Mancia. Effects of chronic clonidine administration on sympathetic nerve traffic and baroreflex function in heart failure. *Hypertension* 38:286–291, 2001. doi:10.1161/hy1201.096117.

[11]Grossmann, A., R. Kronland-Martinet, and J. Morlet. Reading and understanding continuous wavelets transforms. In: Wavelets, Time-Frequency Methods and Phase Space, edited by J. M. Combes, A. Grossmann, and P. Tchamitchian. Berlin: Springer, 1989, pp. 2–20.

[12]Guyton, A. C., T. G. Coleman, and H. J. Granger. Circulation: overall regulation. *Annu. Rev. Physiol.* 34:13–46, 1972. doi:10.1146/annurev.ph.34.030172.000305.

[13]Hayano, J., J. A. Taylor, S. Mukai, A. Okada, Y. Watanabe, K. Takata, and T. Fujinami. Assessment of frequency shifts in R-R interval variability and respiration with complex demodulation. *J. Appl. Physiol.* 77:2879–2888, 1994.

[14]Ichinose, M., M. Saito, N. Kondo, and T. Nishiyasu. Time-dependent modulation of arterial baroreflex control of muscle sympathetic nerve activity during isometric exercise in humans. *Am. J. Physiol. Heart Circ. Physiol.* 290:H1419–H1426, 2006. doi:10.1152/ajpheart.00847.2005.

[15]Ikeda, Y., T. Kawada, M. Sugimachi, O. Kawaguchi, T. Shishido, T. Sato, H. Miyano, W. Matsuura, J. Alexander, Jr., and K. Sunagawa. Neural arc of baroreflex optimizes dynamic pressure regulation in achieving both stability and quickness. *Am. J. Physiol. Heart Circ. Physiol.* 271:H882–H890, 1996.

[16]Jordan, J., H. R. Toka, K. Heusser, O. Toka, J. R. Shannon, J. Tank, A. Diedrich, C. Stabroth, M. Stoffels, R. Naraghi, W. Oelkers, H. Schuster, H. P. Schobel, H. Haller, and F. C. Luft. Severely impaired baroreflex-buffering in patients with monogenic hypertension and neurovascular contact. *Circulation* 102:2611–2618, 2000.

[17]Kashihara, K. Automatic regulation of hemodynamic variables in acute heart failure by a multiple adaptive predictive controller based on neural networks. *Ann. Biomed. Eng.* 34:1846–1869, 2006. doi:10.1007/s10439-006-9190-9.

[18]Kashihara, K., T. Kawada, M. Li, M. Sugimachi, and K. Sunagawa. Bezold-Jarisch reflex induced by phenylbiguanide lowers arterial pressure mainly via the downward shift of the baroreflex neural arc. *Jpn. J. Physiol.* 54:395–404, 2004. doi:10.2170/jjphysiol.54.395.

[19]Kashihara, K., T. Kawada, K. Uemura, M. Sugimachi, and K. Sunagawa. Adaptive predictive control of arterial blood pressure based on a neural network during acute hypotension. *Ann. Biomed. Eng.* 32:1365–1383, 2004. doi:10.1114/B:ABME.0000042225.19806.34.

[20]Kashihara, K., T. Kawada, Y. Yanagiya, K. Uemura, M. Inagaki, H. Takaki, M. Sugimachi, and K. Sunagawa. Bezold-Jarisch reflex attenuates dynamic gain of baroreflex neural arc. *Am. J. Physiol. Heart Circ. Physiol.* 285:H833–H840, 2003.

[21]Kashihara, K., Y. Takahashi, K. Chatani, T. Kawada, C. Zheng, M. Li, M. Sugimachi, and K. Sunagawa. Intravenous angiotensin II does not affect dynamic baroreflex characteristics of the neural or peripheral arc. *Jpn. J. Physiol.* 53:135–143, 2003. doi:10.2170/jjphysiol.53.135.

[22]Kawada, T., T. Miyamoto, K. Uemura, K. Kashihara, A. Kamiya, M. Sugimachi, and K. Sunagawa. Effects of neuronal norepinephrine uptake blockade on baroreflex neural and peripheral arc transfer characteristics. *Am. J. Physiol. Regul. Integr. Comp. Physiol.* 286:R1110–1120, 2004. doi:10.1152/ajpregu.00527.2003.

[23]Kawada, T., Y. Yanagiya, K. Uemura, T. Miyamoto, C. Zheng, M. Li, M. Sugimachi, and K. Sunagawa. Input-size dependence of the baroreflex neural arc transfer characteristics. *Am. J. Physiol. Heart Circ. Physiol.* 284:H404–H415, 2003.

[24]Kent, B. B., J. W. Drane, B. Blumenstein, and J. W. Manning. A mathematical model to assess changes in the baroreceptor reflex. *Cardiology* 57:295–310, 1972.

[25]Landesberg, G., D. Adam, Y. Berlatzky, and S. Akselrod. Step baroreflex response in awake patients undergoing carotid surgery: time- and frequency-domain analysis. *Am. J. Physiol.* 274:H1590–H1597, 1998.

[26]Lee, D. Coherent oscillations in neuronal activity of the supplementary motor area during a visuomotor task. *J. Neurosci.* 23:6798–6809, 2003.

[27]Lipman, R. D., J. K. Salisbury, and J. A. Taylor. Spontaneous indices are inconsistent with arterial baroreflex gain. *Hypertension* 42:481–487, 2003. doi:10.1161/01.HYP.0000091370.83602.E6.

[28]Liu, H. K., S. J. Guild, J. V. Ringwood, C. J. Barrett, B. L. Leonard, S. K. Nguang, M. A. Navakatikyan, and S. C. Malpas. Dynamic baroreflex control of blood pressure: influence of the heart vs. peripheral resistance. *Am. J. Physiol. Regul. Integr. Comp. Physiol.* 283:R533–R542, 2002.

[29]Lucini, D., M. Pagani, G. S. Mela, and A. Malliani. Sympathetic restraint of baroreflex control of heart period in normotensive and hypertensive subjects. *Clin. Sci. (Lond.)* 86:547–556, 1994.

[30]Malliani, A., M. Pagani, F. Lombardi, and S. Cerutti. Cardiovascular neural regulation explored in the frequency domain. *Circulation* 84:482–492, 1991.

[31]Marmarelis, P. Z., and V. Z. Marmarelis. The white noise method in system identification. In: Analysis of Physiological Systems. New York: Plenum, 1978, pp. 131–221.

[32]Masaki, H., T. Imaizumi, Y. Harasawa, and A. Takeshita. Dynamic arterial baroreflex in rabbits with heart failure induced by rapid pacing. *Am. J. Physiol.* 267:H92–H99, 1994.

[33]Mohrman, D. E., and L. J. Heller. Cardiovascular Physiology. 4th ed. New York: McGraw-Hill, 1997.

[34]Motard, R. L., and B. Joseph. Wavelet Applications in Chemical Engineering. Boston: Kluwer Academic Publishers, 1994.

[35]Munakata, M., Y. Imai, H. Takagi, M. Nakao, M. Yamamoto, and K. Abe. Altered frequency-dependent characteristics of the cardiac baroreflex in essential hypertension. *J. Auton. Nerv. Syst.* 49:33–45, 1994. doi:10.1016/0165-1838(94)90018-3.

[36]Osculati, G., G. Grassi, C. Giannattasio, G. Seravalle, F. Valagussa, A. Zanchetti, and G. Mancia. Early alterations of the baroreceptor control of heart rate in patients with acute myocardial infarction. *Circulation* 81:939–948, 1990.

[37]Parati, G., M. DiRienzo, and G. Mancia. Dynamic modulation of baroreflex sensitivity in health and disease. *Ann. NY Acad. Sci.* 940:469–487, 2001.

[38]Parati, G., J. P. Saul, and P. Castiglioni. Assessing arterial baroreflex control of heart rate: new perspectives. *J. Hypertens.* 22:1259–1263, 2004. doi:10.1097/01.hjh.0000125469.35523.32.

[39]Parmer, R. J., J. H. Cervenka, and R. A. Stone. Baroreflex sensitivity and heredity in essential hypertension. *Circulation* 85:497–503, 1992.

[40]Persson, P. B., M. DiRienzo, P. Castiglioni, C. Cerutti, M. Pagani, N. Honzikova, S. Akselrod, and G. Parati. Time versus frequency domain techniques for assessing baroreflex sensitivity. *J. Hypertens.* 19:1699–1705, 2001. doi:10.1097/00004872-200110000-00001.

[41]Pinna, G. D., R. Maestri, G. Raczak, and M. T. La Rovere. Measuring baroreflex sensitivity from the gain function between arterial pressure and heart period. *Clin. Sci. (Lond.)* 103:81–88, 2002.

[42]Pitzalis, M. V., F. Mastropasqua, A. Passantino, F. Massari, L. Ligurgo, C. Forleo, C. Balducci, F. Lombardi, and P. Rizzon. Comparison between noninvasive indices of baroreceptor sensitivity and the phenylephrine method in post-myocardial infarction patients. *Circulation* 97:1362–1367, 1998.

[43]Porta, A., G. Baselli, O. Rimoldi, A. Malliani, and M. Pagani. Assessing baroreflex gain from spontaneous variability in conscious dogs: role of causality and respiration. *Am. J. Physiol. Heart Circ. Physiol.* 279:H2558–H2567, 2000.

[44]Radaelli, A., L. Bernardi, F. Valle, S. Leuzzi, F. Salvucci, L. Pedrotti, E. Marchesi, G. Finardi, and P. Sleight. Cardiovascular autonomic modulation in essential hypertension. Effect of tilting. *Hypertension* 24:556–563, 1994.

[45]Rudas, L., A. A. Crossman, C. A. Morillo, J. R. Halliwill, K. U. Tahvanainen, T. A. Kuusela, and D. L. Eckberg. Human sympathetic and vagal baroreflex responses to sequential nitroprusside and phenylephrine. *Am. J. Physiol.* 276:H1691–H1698, 1999.

[46]Sagawa, K. Baroreflex control of systemic arterial pressure and vascular bed. In: Handbook of Physiology. The Cardiovascular System. Peripheral Circulation and Organ Blood Flow, sect. 2, vol. III, pt. 2, chap. 14. Bethesda, MD: Am. Physiol. Soc., 1983, pp. 453–496.

[47]Sato, T., T. Kawada, M. Inagaki, T. Shishido, H. Takaki, M. Sugimachi, and K. Sunagawa. New analytic framework for understanding sympathetic baroreflex control of arterial pressure. *Am. J. Physiol.* 276:H2251–H2261, 1999.

[48]Sinkkonen, J., H. Tiitinen, and R. Naatanen. Gabor filters: an informative way for analysing event-related brain activity. *J. Neurosci. Methods* 56:99–104, 1995. doi:10.1016/0165-0270(94)00111-S.

[49]Tallon-Baudry, C., O. Bertrand, C. Delpuech, and J. Pernier. Stimulus specificity of phase-locked and non-phase-locked 40 Hz visual responses in human. *J. Neurosci.* 16:4240–4249, 1996.

[50]Toledo, E., O. Gurevitz, H. Hod, M. Eldar, and S. Akselrod. Wavelet analysis of instantaneous heart rate: a study of autonomic control during thrombolysis. *Am. J. Physiol. Regul. Integr. Comp. Physiol.* 284:R1079–R1091, 2003.

[51]Westerhof, B. E., J. Gisolf, J. M. Karemaker, K. H. Wesseling, N. H. Secher, and J. J. van Lieshout. Time course analysis of baroreflex sensitivity during postural stress. *Am. J. Physiol. Heart Circ. Physiol.* 291:H2864–H2874, 2006. doi:10.1152/ajpheart.01024.2005.

[52]Zhang, R., K. Behbehani, C. G. Crandall, J. H. Zuckerman, and B. D. Levine. Dynamic regulation of heart rate during acute hypotension: new insight into baroreflex function. *Am. J. Physiol. Heart Circ. Physiol.* 280:H407–H419, 2001.

Journal of Computational Science and Technology

Vol.3, No.1, 2009

Study on Compressibility Control of Hyperelastic Material for Homogenization Method Using Mixed Finite Element Analysis*

Jun-ichi OKADA** and Toshiaki HISADA***

** Graduate School of Frontier Sciences, University of Tokyo,
5-1-5 Kashiwanoha, Kashiwa, Chiba 277-8563, Japan
E-mail: okada@sml.k.u-tokyo.ac.jp

*** Graduate School of Frontier Sciences, University of Tokyo,
7-3-1 Hongo, Bunkyo-ku, Tokyo, 113-0031, Japan
E-mail: hisada@mech.t.u-tokyo.ac.jp

Abstract

It is well known that the compressibility or incompressibility of biological tissue stems from its microscopic structure, which is generally composed of material with varied compressibility, including incompressibility. This paper proposes a framework for a homogenization method in which the compressibility/incompressibility of the macrostructure properly reflects that of the microstructure. The formulation is based on the mixed variational principle with a perturbed Lagrange-multiplier. It is shown that the rate of volumetric change of the macrostructure can be controlled through the homogenization procedure by introducing the constraint on the microstructure only. A couple of numerical examples are given to demonstrate the validity of the proposed method. By comparing the numerical results with theoretical solutions, the method is also confirmed to be free from locking.

Key words : Homogenization Method, Mixed Finite Element Analysis, Incompressible Materials, Compressible Materials, Hyper-Elasticity, Heart

1. Introduction

The homogenization method is a mathematical modeling technique for efficiently analyzing inhomogeneous material with a periodic microstructure. To measure the change in the spatial domain, we introduce two scales, namely, a scale for the microunit, and a scale for the whole material. By solving the governing equations of both scales with coupling, we can obtain the macroscopic characteristic as an equivalent homogeneous body and variable distribution in the microstructure. To investigate the effect of intracellular structure on heartbeat, we are developing the necessary finite element method in which the heart is analyzed as the macrostructure, and the cardiomyocyte as the microstructure.

In biomaterial, the periodicity hypothesized in the homogenization method is not strictly established. However, Terada et al.[1] have shown that an appropriate equivalent characteristic is obtained in material with an irregular microstructure, if the periodic boundary condition is applied. Thus it is possible to evaluate the effect of each component in the microstructure on the macroscopic behavior, if the microstructure modeling is appropriate. The homogenization method for biomaterial has been applied to bone by Hollister et al.[2], while a two-dimensional analysis of engineered tissue cells has been conducted by Breuls et al.[3]. In an example using the heart, Wanda et al.[4] have applied an excitation propagation phenomena.

Biomaterial is usually modeled by hyperelastic material. However, the myofibril in the cardiomyocyte generates contraction forces and stiffness changed by chemical reaction and includes anisotropic high nonlinearity. In addition, the organization of cytoplasm, mitochondria, nucleus, microtubule, and so on are different intra-cellularly and these also have different

*Received 20 Nov., 2008 (No.T1-07-0579)
Japanese Original: Trans. Jpn. Soc. Mech. Eng., Vol.73, No.735, A (2007), pp.1201–1208 (Received 20 June, 2007)
[DOI: 10.1299/jcst.3.89]

Young and bulk moduli. To treat such material in an unified way, a mixed finite element method based on the perturbed Lagrange-multiplier method is suitable[5]. Although the displacement finite element method is used with only displacement as the unknown independent variable, the characteristic of the mixed finite element method treats pressure as an unknown independent variable in addition to the displacement. A few studies have been reported using a mixed finite element method for homogenization. Yamamoto et al.[6] showed a formulation in which the compressibility control condition is imposed as a penalty method by eliminating the pressure variables analytically. Heguri et al.[7][8] reported a formulation which applied the Perturbed/Augmented Lagrange-multiplier method to the compressibility control condition, where it is assumed that the existence of a solution with an asymptotic expansion type also applies to the pressure. Recently, to extend the formulation of Heguri et al. to anisotropic material, Matsui et al.[9] attempted a Mixed Finite Element formulation in an infinitesimal deformation problem based on the generalized convergence theory. In the formulations by Heguri and Yamamoto, the pressure in the microstructure is also defined, and an incompressibility condition is given, thus achieving the incompressibility condition of the macroscopic structure. However, the theoretical background and process of numerical realization have not been clear.

The purpose of this study, is to formulate a homogenization method for hyperelastic material using mixed finite element analysis based on two-scale convergence theory[10], while considering the compressibility control and process of numerical realization. As described below, this is achieved using two-scale convergence theory in that the rate of volumetric change of the macrostructure can be controlled by the volume average of the volumetric change of the microstructure corresponding to a point of the macrostructure. From this relationship, the compressibility control condition of the microstructure is considered to be a sufficient condition for the compressibility control of the macrostructure and it is also confirmed under finite element discretization.

2. Nomenclature

$\mathbf{Y}, \mathbf{y}$	:position vectors before and after deformation in the microstructure
$\mathbf{X}, \mathbf{x}$	:position vectors before and after deformation in the macrostructure
$\mathbf{u}$	:macroscopic displacement vector
$\mathbf{w}$	:periodic component of the microscopic displacement vector
$\mathbf{F}$	:the deformation gradient tensor
$\mathbf{Z}$	:the displacement gradient tensor
$\mathbf{E}$	:the Green-Lagrange strain tensor
$\mathbf{\Pi}$	:the first Piola-Kirchhoff stress tensor
$\mathbf{I}$	:the identity tensor
I_c, II_c, III_c	:principal invariants
J	:det $\mathbf{F}$

3. Homogenization Method for the Finite Deformation Problem

3.1. Problem Statement and Geometric Prospect

We assume that the material in the body(Ω) reveals heterogeneity on a very fine scale and is characterized by the periodic distribution of a basic structural element(Y_0) as shown in Fig. 1. The following assumptions of homogenization are employed in the formulation of the homogenization method.

- A macrostructure that consists of a periodic microstructure can be considered to be an approximately equivalent homogeneous substance.
- A microstructure is infinitely fine compared with a macrostructure; the variable defined

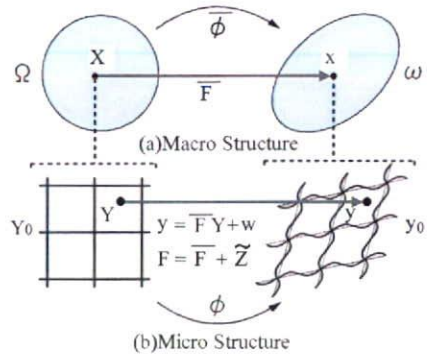

Fig. 1 Homogenization Method in Large Deformation Problem

at each point of the macrostructure corresponds to the volume average of the variables in the microstructure.

To measure the changes in the spatial domains, we introduce two scales: a macro-scale $X \in \Omega$ and a micro-scale $Y \in Y_0$. Thus these scales are characterized by

$$\mathbf{Y} = \mathbf{X}/\epsilon, \tag{1}$$

where ϵ represents the ratio of the two scales. Thus the actual domain can be regarded as the product space $(\Omega \times Y_0)$.

The physical value φ defined in Ω^ϵ is a function dependent on ϵ and is represented by $\varphi^\epsilon(\mathbf{X})$ using ϵ. This can be written as

$$\varphi^\epsilon(\mathbf{X}) = \varphi(\mathbf{X}, \mathbf{X}/\epsilon) = \varphi(\mathbf{X}, \mathbf{Y}) \quad in \quad \Omega \times Y_0, \tag{2}$$

where $\mathbf{X}$ and $\mathbf{Y}$ are independent variables in the micro- and macro-scales, respectively[11]. In the subsequent discussion, a macroscopic quantity defined in Ω corresponding to the microscopic one is expressed by adding a bar symbol over the microscopic symbol.

$\phi : Y_0 \rightarrow y_0$ represents the deformation of the microstructure Y_0. This ϕ maps a point $Y \in Y_0$ of the reference configuration onto a corresponding point $y = \phi(Y) \in y_0$ of the current configuration. The associated gradient map of deformation is expressed by $\mathbf{F} = \nabla_Y \mathbf{y}$ and is called the deformation gradient. To indicate components of tensors, we use an orthogonal coordinate system. For instance, $F_{iJ} = y_{i,J} = \partial y_i / \partial Y_J$. The deformation of the microstructure is assumed to be linked to the local values of the macro continuum via

$$\mathbf{y} = \overline{\mathbf{F}}\mathbf{Y} + \mathbf{w}, \tag{3}$$

where $\mathbf{y}$ and $\mathbf{Y}$ are position vectors defined on the microstructure. Briefly, the deformation of the microstructure is assumed to be composed of a homogeneous part $\overline{\mathbf{F}}\mathbf{Y}$, in which $\overline{\mathbf{F}}$ is constant in the microstructure, and a non-homogeneous superimposed periodic field $\mathbf{w}$, usually referred to as the fluctuation field. As illustrated in Fig. 1(b), the deformed thin-line quadrilateral is the homogeneous deformation caused by the macroscopic deformation gradient, and onto it a fluctuation is superimposed. Consequently, the following relationships

$$\mathbf{F} = \nabla_Y \mathbf{y} = \frac{\partial \mathbf{y}}{\partial \mathbf{Y}} = \overline{\mathbf{F}} + \tilde{\mathbf{Z}}, \tag{4}$$

$$\overline{\mathbf{F}} = \nabla_X \mathbf{x} = \frac{\partial \mathbf{x}}{\partial \mathbf{X}}, \tag{5}$$

$$\tilde{\mathbf{Z}} = \nabla_Y \mathbf{w} = \frac{\partial \mathbf{w}}{\partial \mathbf{Y}}. \tag{6}$$

exist between the microscopic and macroscopic deformation gradients. Thus increment and variation of the deformation gradients become

$$\Delta\mathbf{F} = \Delta\overline{\mathbf{F}} + \Delta\tilde{\mathbf{Z}} = \nabla_X \Delta\overline{\mathbf{u}} + \nabla_Y \Delta\mathbf{w} \tag{7}$$

$$\delta\mathbf{F} = \delta\overline{\mathbf{F}} + \delta\tilde{\mathbf{Z}} = \nabla_X \delta\overline{\mathbf{u}} + \nabla_Y \delta\mathbf{w} \tag{8}$$

For the assumptions mentioned above, the macroscopic gradients are related via the volume averages

$$\overline{\mathbf{F}} = \frac{1}{|V|}\int_{Y_0} \mathbf{F}dY = \frac{1}{|V|}\int_{Y_0}(\overline{\mathbf{F}} + \tilde{\mathbf{Z}})dY = \overline{\mathbf{F}} + \frac{1}{|V|}\int_{Y_0}\tilde{\mathbf{Z}}dY, \tag{9}$$

where V is the volume of the microstructure Y_0. Then, the fluctuation field $\mathbf{w}$ has to satisfy the constraint

$$\int_{Y_0}\tilde{\mathbf{Z}}dY = \int_{Y_0}\frac{\partial \mathbf{w}}{\partial \mathbf{Y}}dY = \int_{\partial Y_0}\mathbf{N}\otimes\mathbf{w}dS = \mathbf{0}. \tag{10}$$

Here, $\mathbf{N}$ is an outward normal vector on the boundary ∂Y_0. This constraint is satisfied when $\mathbf{w}$ is periodic.

3.2. Governing Equation

We now consider the equilibrium of material consisting of a periodic microstructure which is modeled by hyperelastic material. Using the principle of stationary potential energy, the equilibrium condition becomes a functional stationary problem. According to the perturbed Lagrange-multiplier method[5], the total potential energy is defined by the functional

$$\Phi_L^\epsilon = \int_{\Omega^\epsilon} W^\epsilon dV^\epsilon + \int_{\Omega^\epsilon}\lambda^\epsilon\left(U^\epsilon - \frac{\lambda^\epsilon}{\kappa}\right)dV^\epsilon + \int_{\partial\Omega^\epsilon}\mathbf{t}\cdot\mathbf{u}^\epsilon dS^\epsilon, \tag{11}$$

where λ is a Lagrange-multiplier corresponding to $-\frac{1}{2}$ of the pressure and which can be considered as two-field variational problems about λ and u. W^ϵ is the energy function for the deviatric elastic response defined by the deviatric part of the deformation gradient ($\mathbf{F}J^{-\frac{1}{3}}$). On the other hand, U^ϵ is the energy function for the volumetric elastic response and is defined by J. $U(J) = 0$, when $J = 1$. κ is the penalty coefficient for volume change control and compressibility can be controlled using this value. The incompressibility condition can be achieved completely as $\kappa \to \infty$. $\mathbf{t}$ is the traction force and we assume a conservative force. The homogenization method for hyperelastic material can thus be reduced to solving the stationary problem of the above functional under the assumption of homogenization. The stationary condition becomes

$$\delta\Phi_L^\epsilon = \int_{\Omega^\epsilon}\left(\delta\mathbf{F}^\epsilon : \mathbf{\Pi}^\epsilon + \delta\lambda^\epsilon\left(U^\epsilon - \frac{2\lambda^\epsilon}{\kappa}\right)\right)dV^\epsilon + \int_{\partial\Omega^\epsilon}\mathbf{t}\cdot\delta\mathbf{u}^\epsilon dS^\epsilon = 0, \tag{12}$$

$$\mathbf{\Pi}^\epsilon = \mathbf{\Pi}_{dev}^\epsilon + \mathbf{\Pi}_{vol}^\epsilon = \frac{\partial W^\epsilon}{\partial \mathbf{F}^\epsilon} + \frac{\partial U^\epsilon}{\partial \mathbf{F}^\epsilon}\lambda^\epsilon. \tag{13}$$

where $\mathbf{\Pi}_{dev}$ is the stress due to the deviatric deformation, and $\mathbf{\Pi}_{vol}$ is the stress due to volume change. To establish the above equation for arbitrary δu^ϵ and $\delta\lambda^\epsilon$, the necessary and sufficient conditions are

$$G_{\delta u^\epsilon} = \int_{\Omega^\epsilon}\delta\mathbf{F}^\epsilon : \mathbf{\Pi}^\epsilon dV^\epsilon + \int_{\partial\Omega^\epsilon}\mathbf{t}\cdot\delta\mathbf{u}^\epsilon dS^\epsilon = 0, \tag{14}$$

$$G_{\delta\lambda^\epsilon} = \int_{\Omega^\epsilon}\delta\lambda^\epsilon\left(U^\epsilon - \frac{2\lambda^\epsilon}{\kappa}\right)dV^\epsilon = 0. \tag{15}$$

Here, Eq. (14) is the equilibrium equation. Because it can also deal with compressible material, Eq. (15) shall be called the compressibility control condition. Thus the pressure p can be described as

$$p^\epsilon = -2\lambda^\epsilon = -\kappa U^\epsilon. \tag{16}$$

3.3. Multi-scale Boundary Value Problem

We adopt the formulation for homogenization based on the two-scale convergence theory proposed by Terada et al.[13].